Journal of Alloys and Compounds 509 (2011) 7210–7215

Contents lists available at ScienceDirect

Journal of Alloys and Compounds

journal homepage: www.elsevier.com/locate/jallcom

Correlation between the chemical composition and the conduction mechanism of barium strontium titanate thin films

Ala'eddin A. Saif*, P. Poopalan

Microfabrication Cleanroom, School of Microelectronic Engineering, University Malaysia Perlis (UniMAP), Kuala Perlis, Perlis 02000, Malaysia

ARTICLE INFO

Article history:
Received 24 February 2011
Received in revised form 8 April 2011
Accepted 10 April 2011
Available online 20 April 2011

Keywords:
Ceramics
Thin films
Sol–gel processes
Dielectric response
Conduction mechanism
Electrochemical impedance spectroscopy

ABSTRACT

Sol–gel barium strontium titanate thin films with different barium-to-strontium (Ba:Sr) values have been fabricated as MFM configurations. The Perovskite phase for the films is confirmed via XRD. In order to correlate the effect of the chemical composition of the films with the conduction mechanism, different AC electrical parameters have been addressed. The results show that the impedance and dielectric constant decrease as Ba content in the film increases, whereas the conductivity shows the opposite variation; this is attributed to the grain size and dipole dynamics. Complex impedance (Z^*) and electric modulus (M^*) planes show three overlapping regions as the response for the bulk, the grain boundaries and the film/electrode interface mechanisms. These mechanisms have been represented by an equivalent circuit. The imaginary component of electric modulus (M'') versus frequency plots, which reveal relaxation peaks that are not observed in the dielectric loss (ε'') plots, and it is found that these peaks are of a non-Debye-type. Furthermore, the frequency dependent conductivity plot shows three regions of conduction processes.

1. Introduction

Ferroelectric barium strontium titanate ($Ba_{1-x}Sr_xTiO_3$) or BST, has been widely investigated in thin film form for microelectronic applications, such as multilayer ceramic capacitors, dynamic random access memories (DRAM) and ferroelectric field effect transistor (FeFET), due to its low-cost synthesis, high dielectric constant and relatively low dielectric loss tangent [1,2].

Barium-to-strontium (Ba:Sr) ratio in BST thin films plays a significant role at the microstructure and electrical properties. The Curie temperature of BST thin films varies through a long range of values depending on the Ba:Sr ratio [3], which in turn controls the phase of the film, i.e., to be in ferroelectric (with tetragonal lattice) or paraelectric (with cubic lattice) phase. Furthermore, the size of BST grains is directly related to the Ba:Sr ratio, as Ba ions increase in the lattice the grain size increases [4,5], however, the grain size is directly related to the grain boundaries area [6]; as a result, the electrical properties of the material change.

The grain boundaries have an essential role in the conduction mechanism and relaxation phenomenon of the material, thus it is necessary to separate the conductivity due to grain boundaries from that of the bulk [7]. A combination of complex impedance and electric modulus planes has been found to be a powerful method to study many of the electrical properties of the materials and the contribution of the bulk, grain boundaries and electrode interface regions on the dielectric relaxation phenomenon [8]. Furthermore, the frequency dependent conductivity and permittivity studies provide information about the ionic transport mechanism of the materials.

Relatively few studies employ impedance spectroscopy to study BST in thin film form. Czekaj et al. reported the impedance behavior of homogeneous $Ba_{0.6}Sr_{0.4}TiO_3$ and inhomogeneous BST thin films on stainless steel substrate [9]. Agarwal et al. studied the electrical conduction of BST in MIS structure under humid conditions [10]. In this work, sol–gel BST thin films with different Ba:Sr ratios are fabricated in a metal–ferroelectric–metal (MFM) configuration. In order to correlate the effect of the chemical composition of the films with the conduction mechanism, AC electrical parameters such as impedance, electric modulus, permittivity and AC conductivity have been addressed.

2. Experimental

Three solutions with proportions of Ba:Sr (50:50, 70:30 and 80:20) were prepared using barium acetate, strontium acetate and titanium (IV) isopropoxide as the starting material, the preparation details for the solutions can be found elsewhere [4]. The solutions were consecutively named as BST50, BST30 and BST20. The solutions were deposited on $Pt/SiO_2/Si$ substrate of an area of 1.5 cm × 2 cm via spin-coater at 5000 rpm for 20 s, followed by baking at 200 °C for 20 min and heating at 500 °C for 30 min in order to vaporize the organic solvent. The deposition and heating processes were repeated until a specific thickness was obtained. Finally, the films were annealed at 800 °C for 1 h in an O_2 atmosphere. In order to measure the film thickness, the films were partially dipped in diluted hydrofluoric acid (HF)

* Corresponding author. Tel.: +60 19 4948919.
E-mail address: alasaif82@hotmail.com (A.A. Saif).

0925-8388/$ – see front matter © 2011 Elsevier B.V. All rights reserved.
doi:10.1016/j.jallcom.2011.04.068

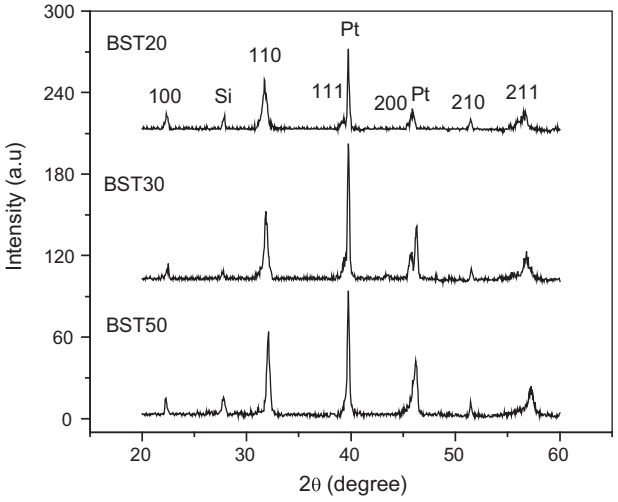

Fig. 1. XRD patterns for various Ba:Sr ratio.

and the resulting step-profile thickness measured with a profilometer. The average thickness of the films is 400 nm.

The crystallization of the films was determined using an X-ray diffractometer (XRD) with a CuKα radiation source (λ = 1.54 Å), operated at a voltage of 40 kV and a current of 40 mA. For impedance measurement, dots of Al with an area of 7.85×10^{-3} cm^2 were deposited on top of the film as the top electrode using a shadow mask via a physical vapor deposition (PVD) technique. The impedance measurements were performed using an impedance gain/phase analyzer (Solartron 1260) in the frequency range of 1 Hz to 1 MHz at room temperature.

3. Results and discussion

3.1. XRD analysis

The XRD patterns of BST50, BST30 and BST20 films, annealed at 800 °C for 1 h are shown in Fig. 1. It can be observed from the figure that the diffraction peaks are (1 0 0), (1 1 0), (1 1 1), (2 0 0), (2 1 0) and (2 1 1) within the 2θ range from 20° to 60°, which confirms that the films are crystallized with a Perovskite structure. The measured lattice parameters of the samples are listed in Table 1. It is observed that the lattice parameters decrease with increasing strontium content; this is attributed to the fact that the ionic radius of Sr is smaller than that of Ba. Table 1 shows that the lattice constants for BST50 are equal, which reveals that it has a simple cubic structure, whereas, for BST30 and BST20 films, the *c*-axis lattice constant is larger than the *a*-axis lattice constant. This suggests that the crystal structure for these films is tetragonal at room temperature.

3.2. Electrical measurements

The variation of the real (Z') and imaginary (Z'') components of impedance with frequency for the films used in this work is shown in Fig. 2(a) and (b), respectively. Fig. 2(a) shows that Z' values decrease with increasing frequency for all BST thin films. Furthermore, it is observed that the values of Z' decrease as the Ba content increases, which is attributed to the grain size effect. The variation of Z'' with frequency reveals a relaxation peak for all BST thin films in the low frequency region; the maximal peak (Z''_{max}) decreases and shifts toward lower frequencies as the Ba content increases. The decreases in Z''_{max} indicate that the conductivity of the films increases, whereas the shifting indicates that as the Ba content increases the relaxation time increases. Prabakar et al. suggested that as the peak shifts to higher frequencies, the measured impedance will equal the static impedance [7]. Furthermore, Fig. 2(b) shows a discontinuity in the Z'' variation at ~2×10^2 Hz for all BST thin films, this attributed to the existence of two different regions in Z''; these regions reveal that different polarization mechanisms occur within BST thin films. In order to further investigate the relaxation mechanisms in BST films, Nyquist plots (Z'' versus Z') are used.

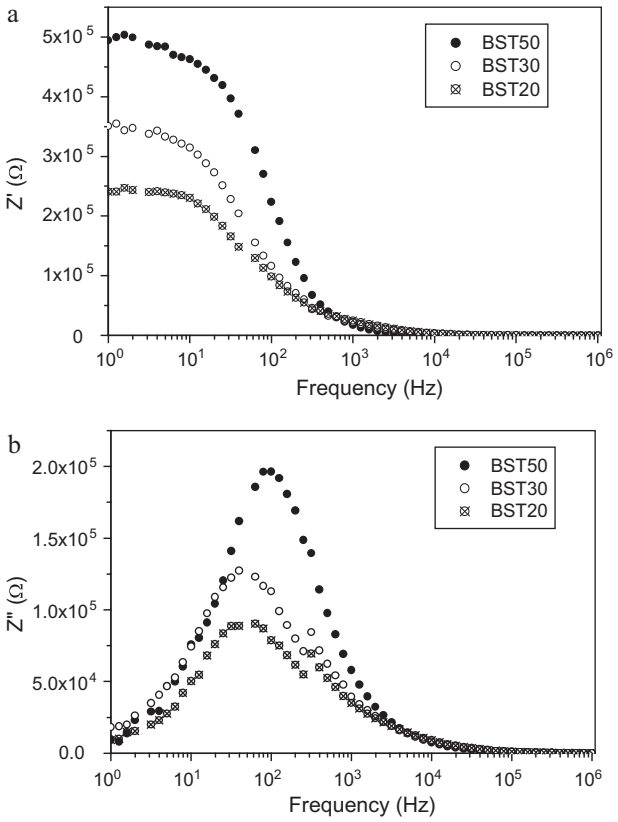

Fig. 2. Variation of real (a) and (b) imaginary components of impedance as a function of frequency for various Ba:Sr ratio at room temperature.

Table 1
Lattice parameters of BST50, BST30 and BST20 films.

Sample	*a* (Å)	*c* (Å)	*c*/*a*	Structure phase
BST50	3.9471	3.9471	1	Simple cubic
BST30	3.9771	3.9883	1.003	Tetragonal
BST20	3.9785	4.0173	1.0098	Tetragonal

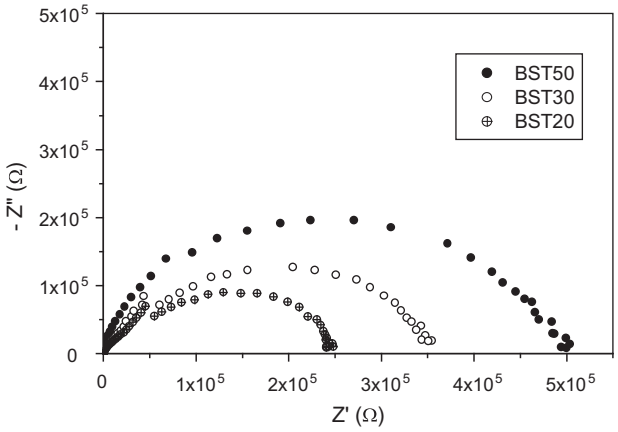

Fig. 3. Nyquist plots for various Ba:Sr ratio at room temperature.

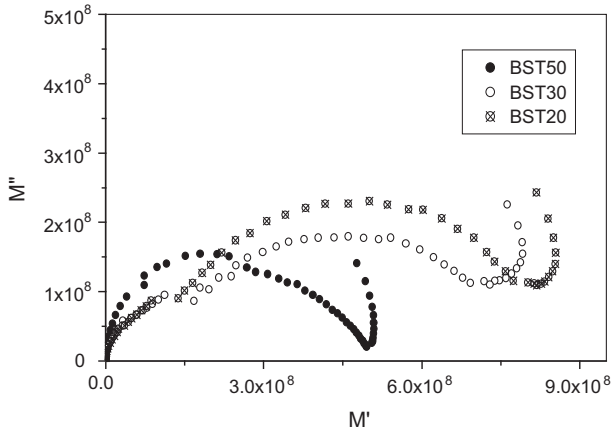

Fig. 4. Electric modulus complex plane for various Ba:Sr ratio at room temperature.

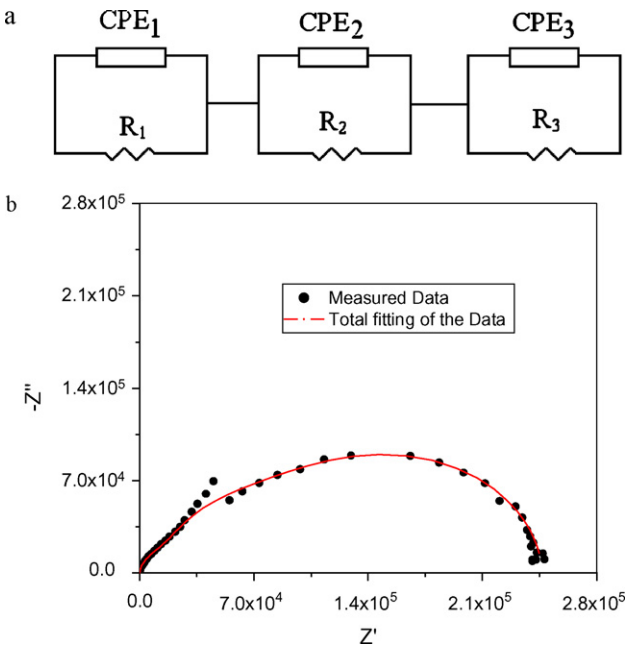

Fig. 5. (a) Suggested equivalent circuit and (b) fitting curve for the BST20 film (the subscripts 1, 2, and 3 represent the bulk, grain boundaries, and electrode, respectively).

Fig. 3 shows that the complex impedance (Z^*) plane for all BST thin films possesses two regions, which indicates that different polarization mechanisms exist within the films. At high frequencies, the figure shows a semicircular arc, which is attributed to the electrical properties of a parallel combination of bulk resistance and capacitance of the BST thin films. At intermediate and low frequencies, the complex impedance plot for all ratios shows two overlapped semicircular arcs, which is attributed to the distribution of the grain boundaries and the film/electrode interface mechanisms, respectively. The overlapping of these arcs suggests distributions of various relaxation times from various grain boundaries and film/electrode interfaces of the BST films.

From Figs. 2 and 3 it can be observed that the total impedance of the films decreases as Sr content decreases. The increment in the bulk and grain boundaries resistance is attributed to the conduction mechanism at the grain–grain boundaries. During the heat treatment for the films in an oxygen atmosphere, oxygen atoms accumulate at the interfaces, creating many electron traps at the grain boundary surfaces [11], as a result, the interfaces trap electrons from the adjacent grains. These electrons cross over the grain barrier and flow into the grain boundary layers, filling the traps first, and then accumulating at the grain boundary interfaces, forming spatial charges [11,12]. However, as the grain size decreases, the number of charge carriers reduces due to the continued electron loss to the grain boundaries. On the other hand, a previous study shows that the grain size of BST increases as the Ba content increases [4,5]. Which indicates that BST50 in this work has the smallest grains; therefore, BST50 has the highest bulk resistance. Furthermore, as the grain size decreases the area of the grain boundaries and electrode interfaces increase, and this leads to an increase in the grain boundaries-electrode resistance due to the increase of the spatial charge density.

In order to resolve the overlapping of the polarization mechanisms for the bulk, grain boundaries, and film/electrode interface in the Nyquist plots, the electric modulus planes of the tested films over the same frequency range are plotted in Fig. 4. The M^* plot for all the films show a minor up-turn at high frequencies, which can be attributed to the bulk due to the frequency range and it appears in the Nyquist plot as a semicircular arc. Further increments in frequency are not possible due to hardware limits. However, at low and intermediate frequencies, BST50 shows two overlapped semicircular arcs, which confirms that the Z^* plot for BST50 in this range of frequencies consists of two overlapping regions, whereas BST30 and BST20 films show an arc and a semicircle overlapping together; these features are attributed to the film/electrode interface and grain boundaries, respectively. The well distinguishable regions for BST30 and BST20 could be attributed to the permanent dipoles existing in their lattice, since these films are crystallized with a tetragonal structure as was discussed in the XRD subsection. Whereas, the BST50 lattice lacks this kind of dipole since it is crystallized with a cubic structure.

In order to analyze and interpret the impedance spectrum, it is useful to have an equivalent circuit model that provides a realistic representation of the electrical properties of the respective regions; therefore, each semicircle is represented by a parallel RC element [9,13]. However, it is observed that the measured capacitance response of BST in the whole frequency range is not ideal, i.e., BST does not behave as a pure capacitor; this can be attributed to the distribution of the various relaxation times. This deviation is solved by using a constant-phase element (CPE) instead of an ideal capacitor; the impedance of the CPE is given by [14]

$$Z_{\mathrm{CPE}} = \frac{1}{A(j\omega)^n} \tag{1}$$

where A is a fitting parameter that is independent of frequency, ω is the angular frequency, and n is the arc depression factor. In the ideal case where $n = 1$, the CPE works as an ideal capacitor and A in this case will equal the capacitance C [9].

Depending on the Z^* and M^* planes, an equivalent circuit composed of three parallel combinations of resistance (R) and constant phase element (CPE) is suggested, as shown in Fig. 5. The bulk, grain boundaries and electrode effects are represented by the parallel R_1–CPE_1, R_2–CPE_2 and R_3–CPE_3 combinations, respectively. The fitting was performed using Zview impedance analysis software (Scriber Associates, Inc.), for the fitting of the weighted data that used 'calc-Modulus', which gives a good fit due to each data point being weighted by its normalized magnitude [14]. The value of the bulk, grain boundaries or electrode resistance (R) in the equivalent circuit is obtained from the fitting of the impedance data. The value of the relaxation frequency ($f_{\max}$) and capacitance (C) are calculated using the following relations [9]:

$$f_{\max} = \frac{1}{2\pi(RA)^{1/n}} \tag{2}$$

Table 2
The estimated values of the equivalent circuits' parameters.

Parameter	BST50	BST30	BST20
R_1 (Ω)	43,900	11,900	9600
C_1 (F)	2.27×10^{-9}	1.8×10^{-8}	4.84×10^{-8}
f_{1max} (Hz)	1600	742	343
R_2 (Ω)	320,000	248,000	160,000
C_2 (F)	3.8×10^{-9}	6.13×10^{-9}	1.1×10^{-8}
f_{2max} (Hz)	131	104.7	90
R_3 (Ω)	150,000	98,000	82,000
C_3 (F)	1.65×10^{-8}	4.78×10^{-8}	3.8×10^{-8}
F_{3max} (Hz)	64.5	34	51.2

$$C = \frac{1}{2\pi R f_{max}} \quad (3)$$

where f_{max} is the relaxation frequency and C is the capacitance of the bulk, grain boundaries or electrode. The fitted values of the equivalent circuits' parameters are listed in Table 2. From the table it can be observed that the bulk resistance is much less than the grain boundary resistance, which indicates that the bulk has a more important effect on the conduction mechanism than the grain boundaries, in agreement with the results obtained in Fig. 3.

The study of the dielectric properties is another important source of valuable information about conduction processes since it can be used to understand the origin of the dielectric losses, the electrical and dipolar relaxation time [15]. For this matter, the dielectric permittivity was determined from the measured values of the impedance using the following relations [16]:

$$\varepsilon^* = \varepsilon' - j\varepsilon'' = \frac{-Z'}{(Z'^2 + Z''^2)\omega C_0} + \frac{-Z''}{(Z'^2 + Z''^2)\omega C_0} \quad (4)$$

where C_0 is the capacitance in the free space.

Fig. 6(a) shows the frequency dependent plots of the real part of the dielectric constant (ε') for various Ba:Sr ratio films at room temperature. It is observed that the value of ε' for all Ba:Sr ratios decreases as the frequency increases and attains a constant limiting value, at which ε' becomes almost frequency-independent. The high value of the dielectric constant at low frequencies can be explained as an accumulation of charges at the interfaces between the sample and the electrodes, i.e., Maxwell–Wagner polarization and interfacial polarization [17]. As the frequency increases, the dipoles in the samples cannot reorient themselves fast enough to respond to the applied electric field resulting in the decrease of ε'.

On the other hand, at higher frequencies, it has been observed that the ε' value increases as the Ba content decreases, which is attributed to the decrease in the grain size. Depending on the results obtained from our previous work [4,5], the films contain lower amounts of Ba, and they have a smaller grain size, which implies a larger grain boundary area. However, it can be considered that the grains and the grain boundaries act as an interior capacitors network, since the grains are more conductive compared to the grain boundaries, as can be observed from the fitted value of Z^* planes in Table 2. This implies that the effective capacitance of the film increases as the grain size decreases, due to the increase of the grain boundaries area. As a result, the overall dielectric constant of the film increases with the decrease in the grain size.

Fig. 6(b) shows the frequency dependence of the imaginary part of the dielectric constant (dielectric loss) ε'' for the tested films at room temperature. The same feature for dielectric loss is observed as for the dielectric constant. There are no appreciable relaxation peaks in the frequency range employed in this study. It is believed that the ionic conduction may mask any relaxation mechanism.

The variation of loss tangent ($\tan\delta = \varepsilon''/\varepsilon'$), as a function of frequency, is given in Fig. 7. The figure shows a kink at ~60 Hz for all BST thin films; this kink separates the polarization mechanism occurring due to the electrode effect from the grain boundaries

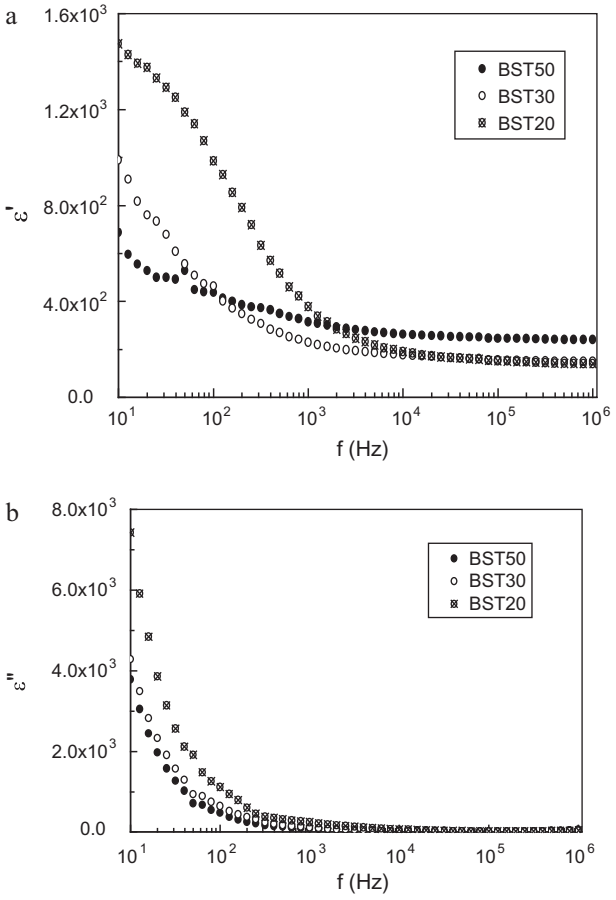

Fig. 6. Variation of (a) ε' and (b) ε'' versus frequency for various Ba:Sr ratio at room temperature.

mechanism, which is not noticeable in the ε'' or ε' plots. However, it is observed that the dispersion process occurring due to the electrode mechanism is stronger than the one resulting from the grain boundaries. A broad peak in BST30 and BST20 is observed. This kind of peak occurs when the hopping frequency of electric charge carriers becomes approximately equal to that of the external applied AC electric field [18], however, this peak becomes more noticeable and shifts toward lower frequencies as the Ba content increases. This could be attributed to the increase of the grain size and dipoles presence.

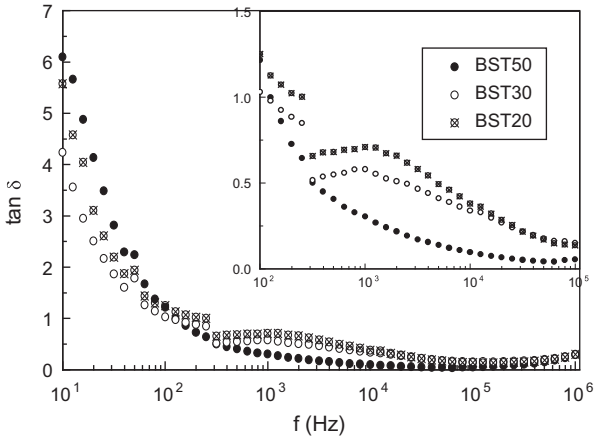

Fig. 7. Variation of the $\tan\delta$ versus frequency for various Ba:Sr ratio at room temperature.

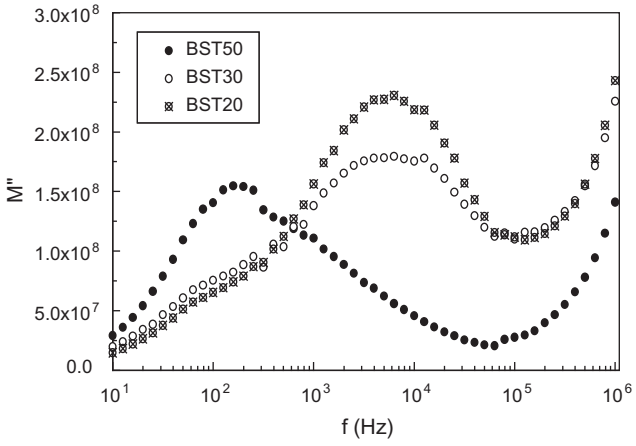

Fig. 8. Variation of the M'' versus frequency for various Ba:Sr ratio at room temperature.

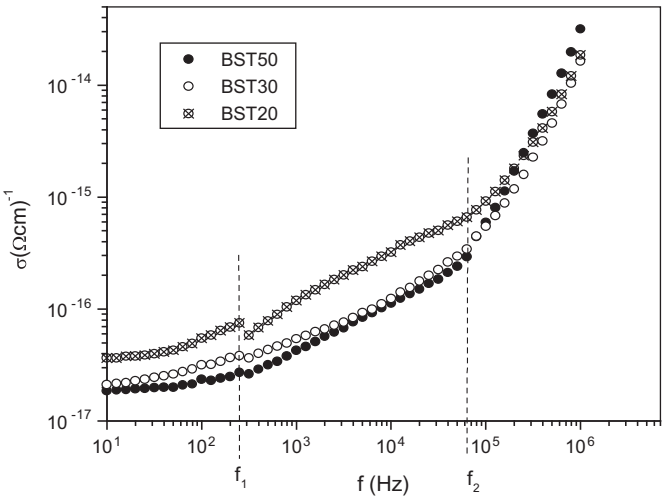

Fig. 9. AC conductivity $\sigma(f)$ as a function of frequency for various Ba:Sr ratio at room temperature.

In order to reveal the relaxation peak in the ε'' plot, the effect of the electrode polarization must be excluded. This can be achieved by following the electric modulus approach, since the electric modulus corresponds to the relaxation on the electric field in the material when the electric displacement remains constant. This approach can be effectively used to separate out the electrode effects that mask the dielectric relaxation.

Fig. 8 shows the variation of the imaginary component of the electric modulus M'' with frequency. It can be seen that M'' for the BST50 film shows a broad peak located in the range of ~50 Hz to 1 kHz; this widening of the peak could be resulting from two overlapped peaks, i.e., the electrode and grain boundaries. Whereas, in BST30 and BST20, M'' shows a low and unclear peak at a low frequency of ~70 Hz, attributed to the electrode effect. However, the grain boundaries peak, which is not well defined for BST50, is transformed to a dominant peak of ~6.4 kHz for these films, which explains the well-defined semicircle observed at intermediate frequencies in the M^* plot. The frequency region below the peak maximum of M'' determines the range in which the charge carriers are mobile over long distances and in the region above the peak maximum the carriers are confined to potential wells being mobile over short distances [19].

The modulus plot can be characterized by full width at half height or in terms of a non-exponential decay function. The stretched exponential function is defined by the empirical Kohlrausch–Williams–Watts (KWW) relationship [20]

$$\phi(t) = e^{(-t/\tau)^{\beta}} \quad 0 < \beta < 1 \tag{5}$$

where τ is the characteristic relaxation time and β is the Kohlrausch parameter, which represents the deviation from a Debye-type relaxation ($\beta = 1$) and it decreases with the increasing of the relaxation time distribution.

The value of the parameter β is calculated by extracting FWHM of the modulus peaks using $\beta = 1.14/\text{FWHM}$. It has been found that the values of β for BST50, BST30 and BST20 films are 0.26, 0.87 and 0.95, respectively. This indicates that the relaxation process for all the tested samples is of a non-Debye-type. Furthermore, the smaller the value of β, the greater the deviation with respect to Debye-type relaxation [19]. However, the low frequency peak in BST30 andBST20 films is considered to be a non-Debye-peak as well since it is too broad.

The study of frequency dependent conductivity is a well-established method for characterizing the hopping dynamics of the charge carrier/ions. Fig. 9 shows a typical frequency dependence of AC conductivity σ for various Ba:Sr ratio films. The frequency dependence of AC conductivity is usually characterized by a power law as given below [21–24].

$$\sigma_{AC} = Xf^{s} \tag{6}$$

where X is a temperature-dependent constant and s is the frequency exponent, which can be determined from the measured results.

It is observed from Fig. 9 that all BST results show two threshold frequencies, f_1 and f_2, separating the entire variation into three regions: (i) Low frequencies region, $f < f_1$, in which the conductivity is almost frequency independent, called σ_{DC}. (ii) Moderate frequencies region, $f_1 < f < f_2$, where the conductivity increases linearly with the frequency. The values of s are obtained by fitting σ versus f plots in this region, which are found to be located between 0.37 and 0.51, i.e. $0 < s < 1$. This reveals that the conduction mechanism in this region corresponds to the translational hopping motion [23,24]. (iii) High frequencies region, $f > f_2$, where the conductivity increases linearly with the frequency. In this region s values vary between 1.38 and 1.77, i.e. $1 < s < 2$. Which reveals that the conduction mechanism in this range of frequencies corresponds to the well-localized hopping and/or reorientational motion [23,24].

At low and intermediate frequencies, Fig. 9 shows that the conductivity increases as Ba content increases; this is attributed to the grain sizes effect. It is mentioned earlier from previous work that the films with less Ba content have smaller grains, which lead to larger grain boundary areas. This in turn gives rise to higher density of the charges accumulated at the interfaces. These charges act to block any mobility for the free carrier, thus, the conductivity of the film decreases as a result. These results agree very well with the impedance results in Figs. 2 and 3. On the other hand, it is observed that at high frequencies, the conductivity of BST50 film shows higher values compared to that of BST30 and BST20 films. This phenomenon can be explained considering the dipole elongation responding to the applied electric field. It is discussed earlier in XRD subsection that BST30 and BST20 films are crystallized in a tetragonal phase which leads that their lattice contains a valuable number of permanent diploes whereas BST50 lacks to this kind of dipoles since it is crystallize with a cubic phase. Furthermore, as an AC electric field is applied at BST lattice, it creates a new dipoles, reorients the permanent dipoles to the direction of the applied filed and causes an induced shift to the Ti ions for the dipoles that are already have the same orientation of the applied field in case of BST30 and BST20 films, which in turn increases their length. However, as the frequency increases, the longer dipoles find it harder to follow the applied field, as a result, lower conductivity is obtained.

4. Conclusion

Perovskite-type $Ba_{1-x}Sr_xTiO_3$thin films with different x values have been fabricated as MFM configurations using a sol–gel method. In order to correlate the effect of the chemical composition of the films with the conduction mechanism, different AC electrical parameters have been addressed. The results show that the impedance and dielectric constants decrease as the Ba content in the film increases, whereas the conductivity shows the opposite, which is attributed to the grain size and dipole dynamics. Z^* and M^* planes show three overlapping regions as responses for the bulk, the grain boundary and the film/electrode interface mechanisms, and an equivalent circuit has been proposed for each mechanism. M'' versus frequency plots reveal relaxation peaks that are not observed in the ε'' plots, and it is found that these peaks are of a non-Debye-type. The frequency dependent conductivity plot shows three regions of conduction processes, i.e., a low-frequency region due to DC conduction, a mid-frequency region due to translational hopping motions and a high-frequency region due to localized hopping and/or reorientational motion.

References

[1] C. Hongwei, Y. Chuanren, F. Chunlin, Z. Li, G. Zhiqiang, Appl. Surf. Sci. 252 (2006) 4171–4177.
[2] G. Li, P. Yu, D. Xiao, J. Electroceram. 21 (2008) 340–343.
[3] T. Mazon, M.A. Zaghete, J.A. Varela, E. Longo, J. Eur. Ceram. Soc. 27 (2007) 3799–3802.
[4] Ala'eddin A. Saif, N. Ramli, P. Poopalan, Jordan J. Phys. 3 (2010) 61–68.
[5] Ala'eddin A. Saif, P. Poopalan, Solid State Electron. (2011), doi:10.1016/j.sse.2011.03.004.
[6] C.K Chung, A. Nautiyal, T.S. Chen, Y.L. Chang, J. Phys. D: Appl. Phys. 41 (2008) 185404.
[7] Sa.K. Prabakar, K. Narayandass, D. Mangalaraj, Mater. Sci. Eng. B 98 (2003) 225231.
[8] Joao C.C. Abrantes, Joao A. Labrincha, Jorge R. Frade, Mater. Res. Bull. 35 (2000) 727–740.
[9] D. Czekaj, A. Lisinska-Czekaj, T. Orkisz, J. Orkisz, G. Smalarz, J. Eur. Ceram. Soc. 30 (2010) 465–470.
[10] S. Agarwal, G.L. Sharma, R. Manchanda, Solid State Commun. 119 (2001) 681–686.
[11] L. Bing-Ce, L. Ci-Hui, F. Zhu-Xi, Y. Bo, Chin. Phys. Lett. 26 (2009) 117101–117104.
[12] A. Alim Mohammad, S. Li, F. Liu, P. Cheng, Phys. Status Solidi (a) 203 (2005) 410–427.
[13] S.G. Song, Z. Ling, F. Placido, Mater. Res. Bull. 40 (2005) 1081–1093.
[14] S.H. Song, P. Xiao, J. Mater. Sci. 38 (2003) 499–506.
[15] R. Ayouchi, D. Leinen, F. Martın, M. Gabas, E. Dalchiele, J.R. Ramos-Barrado, Thin Solid Films 426 (2003) 68–77.
[16] D.K. Pradhan, R.N.P. Choudhary, B.K. Samantaray, Int. J. Electrochem. Sci. 3 (2008) 597–608.
[17] U. Akgul, Z. Ergin, M. Sekerci, Y. Atici, Vacuum 82 (2008) 340–345.
[18] M.A. Elkestawy, S. Abdelkader, M.A. Amer, Physica B 405 (2010) 619–624.
[19] M. Ram, S. Chakrabarti, J. Alloys Compd. 462 (2008) 214–219.
[20] P.S. Anantha, K. Hariharan, Mater. Sci. Eng. B 121 (2005) 12–19.
[21] S. Selvasekarapandian, M. Vijayakumar, Mater. Chem. Phys. 80 (2003) 29–33.
[22] P. Muralidharan, M. Venkateswarlu, N. Satyanarayana, Mater. Chem. Phys. 88 (2004) 138–144.
[23] S. Mahboob, G. Prasad, G.S. Kumar, Bull. Mater. Sci. 29 (2006) 347–355.
[24] A.A. Ahmed, Youssef, Z. Naturforsch. 57a (2002) 263–269.